

# Acoustic emission characteristics and energy mechanism in karst limestone failure under uniaxial and triaxial compression

Qingsong Wang<sup>1</sup> · Jianxun Chen<sup>1</sup> · Jiaqi Guo<sup>1,2</sup> · Yanbin Luo<sup>1</sup> · Hongyu Wang<sup>1,3</sup> · Qin Liu<sup>1</sup>

Received: 20 March 2017 / Accepted: 20 October 2017 / Published online: 6 November 2017  
© Springer-Verlag GmbH Germany 2017

**Abstract** Acoustic emission (AE) tests were performed on saturated karst limestone under uniaxial and triaxial compression. Mechanical properties, AE characteristics, and the energy mechanism of rock failure were analyzed. The peak AE activity under uniaxial compression occurred near the peak stress of the rock. Under triaxial compression, the AE activities of the rock samples first decreased then increased with increases in confining pressure. AE activity exhibited a certain lag, and the peak AE appeared when the stress had decreased significantly. Stratification of the average signal level occurred at low confining pressures. The critical confining pressure was between 15 and 20 MPa, and at this pressure a dramatic change occurred in the AE characteristics of the limestone.

Total strain energy, dissipated energy, and elastic strain energy at peak stress showed good exponential relationships with confining pressure and peak rock strength.

**Keywords** Karst limestone · Uniaxial compression · AE · Triaxial compression · Energy mechanism

## Introduction

Karst disaster is one of the most severe and common geological hazards in the construction of underground structures, such as traffic tunnels, mines, and hydraulic tunnels (Guo et al. 2014). There is a close relationship between the hazard and the surrounding rocks in the karst area. Limestone is widely present in karst areas, and researchers have studied it. Previous studies on limestone have mainly focused on the following aspects.

1. Physical and mechanical properties of rock. The most basic research subjects include density, porosity, water content, and mechanical properties (e.g., compressive strength, tensile strength, elastic modulus, and Poisson's ratio) under different loading conditions.
2. Acoustic emission (AE) characteristics. The AE technique can collect and analyze acoustic waves during rock failure, and the AE characteristics and parameters can well reflect the rock fabric and damage evolution process (Lokajicek et al. 1996; Prikryl et al. 2003; Iturrioz et al. 2013, 2014; Wang et al. 2014). Common parameters include event rate, ring-down counts, energy rate, amplitude, average signal level (ASL) and frequency. Farahat and Ohtsu (1995) studied the relationship between the plastic damage and the AE events in concrete subjected to uniaxial compressive loading, and found that as the

✉ Jianxun Chen  
chenjx1969@chd.edu.cn

Qingsong Wang  
wangqs\_1989@163.com

Jiaqi Guo  
gj519@163.com

Yanbin Luo  
lyb@chd.edu.cn

Hongyu Wang  
whyd1990@163.com

Qin Liu  
chinlau@chd.edu.cn

<sup>1</sup> School of Highway, Chang'an University, Xi'an, Shaanxi 710064, China

<sup>2</sup> School of Civil Engineering, Henan Polytechnic University, Jiaozuo, Henan 454000, China

<sup>3</sup> Shaanxi Provincial Transport Planning Design and Research Institute, Xi'an, Shaanxi 710068, China

plastic damage increases the AE signal activity also increases. Amitrano (2003) analyzed the AE and the mechanical behavior of granite samples under triaxial compression, and found that the size of AE events show power law distributions in accordance with the Gutenberg-Richter law observed for earthquakes, which is characterized by the  $b$  value.

Brantut et al. (2011) conducted triaxial tests on gypsum polycrystal samples at confining pressures ( $P_c$ ) ranging from 2 to 95 MPa and temperatures up to 70 °C. During the tests, stress, strain, elastic wave velocities, and AEs were recorded. They found that at  $P_c \leq 10$  MPa, the macroscopic behavior is brittle, and at  $P_c < 20$  MPa the macroscopic behavior is ductile. Yang et al. (2014) conducted AE tests on limestone under triaxial compression and analyzed the characteristics of damage evolution using AE parameters, and found that confining pressure can cause the decrease of AE activities in compaction stage, and the highest AE ring-down count values occur after macroscopic failure of the specimen.

Liu et al. (2015) studied the AE signal in the recognition of different rocks (granulite, granite, limestone, and siltstone) using wavelet transform and an artificial neural network, and found that different rocks had different rupture features and AE characteristics. Vervoort and Govaerts (2006) studied the Kaiser effect in limestone samples under triaxial compression. Xiao et al. (2013) analyzed the AE features of limestone under uniaxial compression, and established the limestone damage model based on the AE features. Tuncay and Obara (2012) compared stress values obtained from AE and compact conical-ended borehole overcoring stress measurement techniques applied at an underground limestone mine in Japan. Lee and Rathnaweera (2016) studied the deformation and fracturing of Bukit Timah granite in Singapore under uniaxial and triaxial loading conditions. The crack volumetric strain approach has been shown to be a more precise method for identifying crack initiation, and the results of the AE detection technique are consistent with those of the crack volumetric strain approach.

3. Energy mechanism. Rock failure is a process of microcrack initiation, propagation, and coalescence, and it is the net result of energy absorption, dissipation, and release (Xie et al. 2005, 2008; Zhang and Gao 2012; You and Hua 2002; Li et al. 2014). Mikhalyuk and Zakharov (1997) established the general mechanism of variation in the energy capacity of dynamic deformation with variation in loading intensity and conditions based on experiments with various intrusive rocks, and compared qualitative data on the dissipation of dynamic loading energy in the regions of quasielastic and elastoplastic deformation. Zhang et al. (2013) analyzed the energy evolution characteristics of limestone during the entire

deformation process in samples subjected to uniaxial and conventional triaxial compression, and unloading. Tang and Li (2014) and Tian and Yu (2014) studied the energy mechanism of rock failure under triaxial pressure and analyzed the energy change equations for several stages in the compression process with the aim of explaining rock failure modes at high confining pressures. The results revealed linear relationships between peak stress and confining pressure and between Young's modulus and confining pressure.

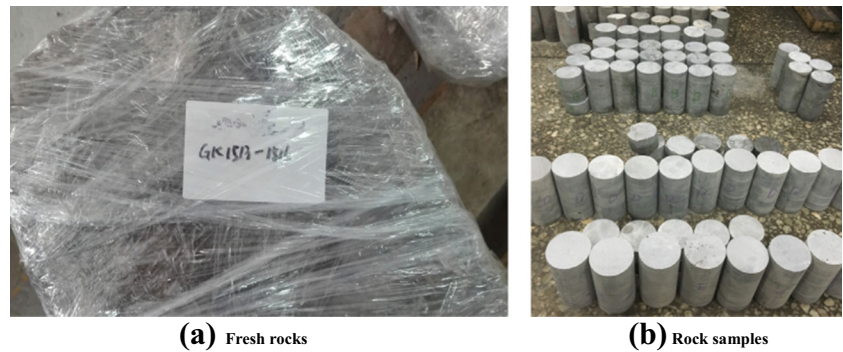
Guo et al. (2014) conducted experiments on natural and saturated karst limestones under uniaxial and triaxial loading and studied the energy features and energy mechanism during failure. Chen et al. (2016) conducted a series of conventional triaxial compression tests on granite from Kirchberg (Saxony, Germany) and performed corresponding numerical simulations to study prefailure damage characteristics, and deduced a new failure criterion based on correlations between maximum elastic strain energy density and uniaxial compressive strength and confining pressure. Huang and Li (2013) conducted axisymmetric triaxial compression loading/unloading tests on marble specimens with different initial confining pressures and different unloading rates, and found that the failure mode gradually changes from shear to tensile with increasing unloading rate. The prepeak conversion rate of strain energy increases with increasing unloading rate. This increase is enhanced by initial confining pressure.

Studies on karst limestones have focused on mechanical properties combined with AE characteristics or on mechanical properties combined with the energy mechanism, but no studies have combined the three aspects. The hazard of water and mud inrush in karst tunnels is closely related to the decrease in rock strength because of the saturated conditions. Therefore, typical karst limestone was chosen for this study and the mechanical properties, AE characteristics, and energy mechanism of the limestone under saturated conditions were investigated in AE experiments. Fracture formation and development and the final failure mode were explored. The aim of the study was to clarify the mechanism of tunnel disasters in karst areas to reduce or prevent their occurrence.

## Experimental methods

### Rock sample preparation

Fresh rocks (about 40 cm × 40 cm × 30 cm) without obvious large-jointed crevices were obtained from the entrance to Qiyueshan Tunnel in Hubei Province, China. The fresh rocks were sealed at the construction site and then transported to the

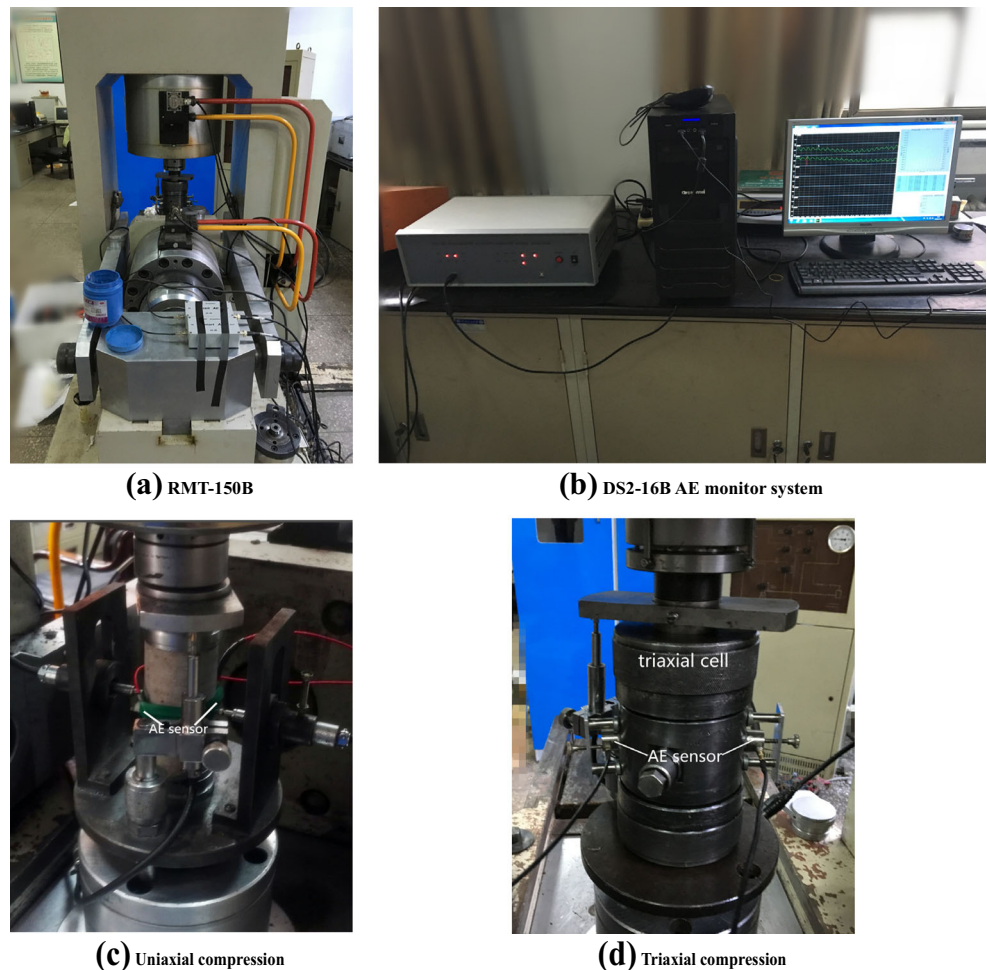
**Fig. 1** Rock sample preparation

laboratory. According to testing standards, the rocks were machined strictly into  $\Phi 50 \text{ mm} \times 100 \text{ mm}$  cylindrical samples (Fig. 1). The free water immersion method was used for saturation.

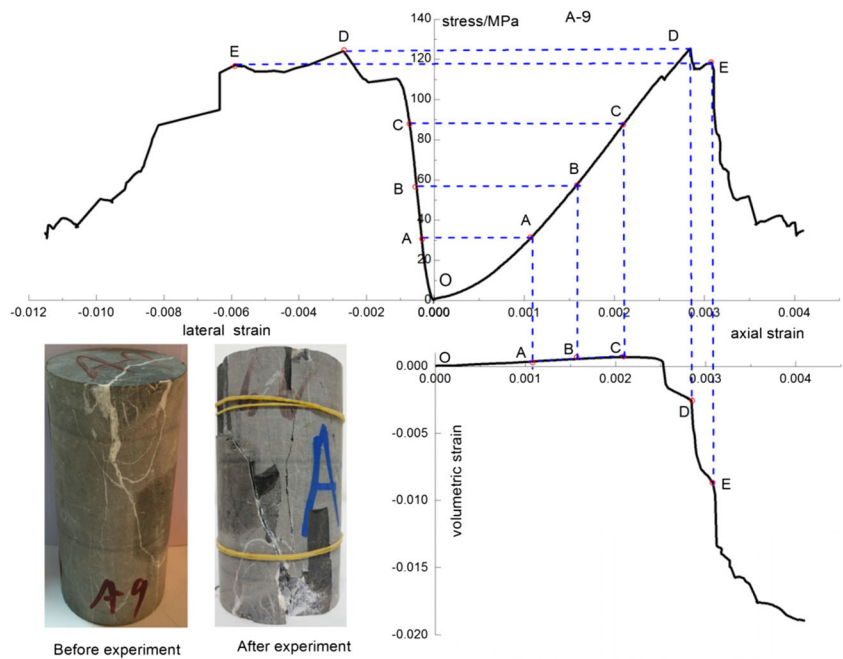
### Equipment and loading conditions

The loading equipment used comprised a RMT-150B computer-controlled triaxial apparatus. The system can provide 1,000 kN of maximum axial load, 20 mm of

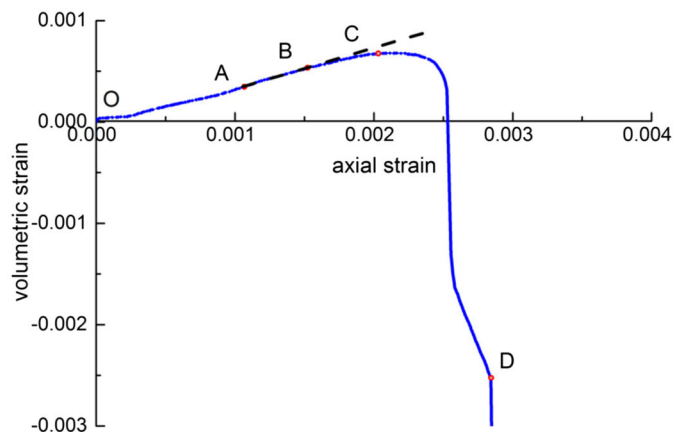
maximum axial displacement, and 50 MPa of maximum confining stress. A DS2-16B AE monitor system was used during the test. The threshold value was set to 50 mV and the preamplifier gain was set to 40 dB as used in previous studies to eliminate the effect of noise on the AE test, and the sampling frequency was set to 3.0 MHz. The loading modes included uniaxial and triaxial compression. For uniaxial compression loading, the displacement control mode was used, and the deformation rate was 0.002 mm/s. AE detection was synchronized with

**Fig. 2** Experimental instruments

**Fig. 3** The whole stress–strain curve of rock under uniaxial compression



**(a)** The whole stress–strain curve of rock under uniaxial compression



**(b)** Larger image of volumetric strain curve

the loading process. As shown in Fig. 2c, two AE sensors were placed symmetrically on the sides of the limestone sample. Petroleum jelly was applied to the contact face as a couplant between the sensor and the sample. Three rock samples were repeated in the uniaxial compression test.

In the triaxial compression test, the confining pressures applied were 5, 10, 15, 20, and 25 MPa. First, the axial stress and confining stress were loaded at the same time. The axial stress loading rate was 1.0 kN/s, and the confining stress loading rate was 0.05 MPa/s. When the confining pressure reached the target value, it was held constant during the test. Triaxial compression was then added with an axial displacement rate of 0.005 mm/s until sample failure. AE was recorded during triaxial compression.

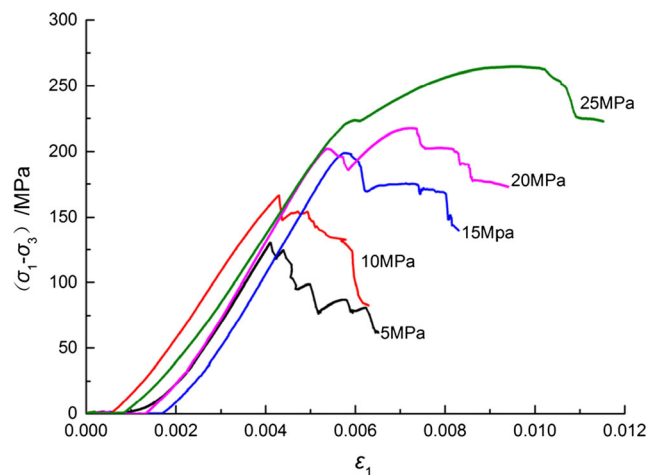


**Fig. 4** Rock stress–strain curves under triaxial compression



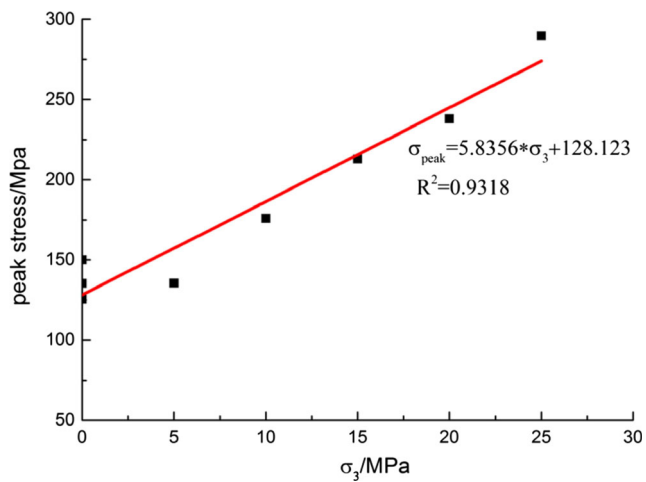


**Fig. 5** Fitting curve of peak stress versus confining pressure

As shown in Fig. 2d, two AE sensors were placed symmetrically on the sides of the triaxial cell. The sensors were fixed onto the triaxial cell using two magnetic pressing blocks with petroleum jelly applied between the block and the cell.

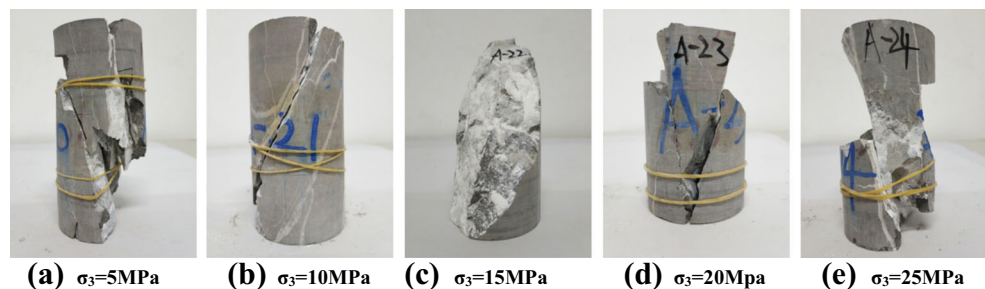
## Mechanical properties and failure characteristics

### Mechanical properties under uniaxial compression

As shown in Fig. 3a, the front peak stress–strain curve of the saturated water sample shows an “S” shape, which is consistent with the stress–strain curve for karst limestone obtained by Li et al. (2007). In this study, the stress–strain relationship of the saturated limestone under uniaxial compression can be divided into the following stages:

1. Initial compression stage (O–A): The native internal fractures close during compression, the stress–strain curve is nonlinear and slightly concave. The stress–volumetric strain and stress–transverse strain are also nonlinear.
2. Elastic deformation stage (A–B): Most fractures have closed, and stress–axial strain, stress–volumetric strain, and stress–transverse strain are all linear. Initially, the cracks increase to a certain length with increasing stress;

**Fig. 6** Forms of rock failure under different confining pressures



(a)  $\sigma_3=5\text{MPa}$

(b)  $\sigma_3=10\text{MPa}$

(c)  $\sigma_3=15\text{MPa}$

(d)  $\sigma_3=20\text{MPa}$

(e)  $\sigma_3=25\text{MPa}$

eventually, the cracks stop increasing, and can then be considered stable (Zhang and Gao 2012; Xiao et al. 2013).

3. Stable fracture growth stage (B–D): In stage B–C, inner rock fractures begin extending, and the volume strain–axial strain curve deviates from linearity. Starting from point C, the rock enters the dilatancy stage. The inner fractures begin to link with one another, and this usually corresponds to the characteristic points of the rotation of the volumetric strain curve.
4. Unstable fracture growth stage (D–E): In this stage, fracture development shows a qualitative change: the stress concentration at the crack tip is obvious, and continuous fracture growth causes stress and energy release. Transverse strain and volumetric strain are both increasing, and a large number of fractures extend and coalesce. A macroscopically fractured surface begins to form.
5. Failure stage (after E): Macroscopic fracture surfaces form, the dilatancy is strong, strength decreases rapidly until the rock breaks completely and loses carrying capacity. Notably, the stress–strain curves of the rock samples exhibit a difference due to the nuances of the internal defects (cracks, pores, and other joints), but they can be analyzed generally as the general pattern of karst limestone deformation and failure. The ultimate failure of the rock is marked by the formation of a coalescent failure surface, and the rock divides into blocks. In the entire deformation process before final failure, both elastic deformation and brush-fire damage occur, which make the inner stress distribution complex (Yang and Zhou 2010).

### Mechanical properties under triaxial compression

As shown in Fig. 4, in the triaxial compression tests, samples are subjected to the compression, elastic and plastic deformation stages, and then entered the softening stage. The samples show more obvious plasticity under confining pressure than under uniaxial compression. When the sample reaches peak stress, the stress curves shows some ductility, which is different from the sharp decline in the stress curves under uniaxial compression.

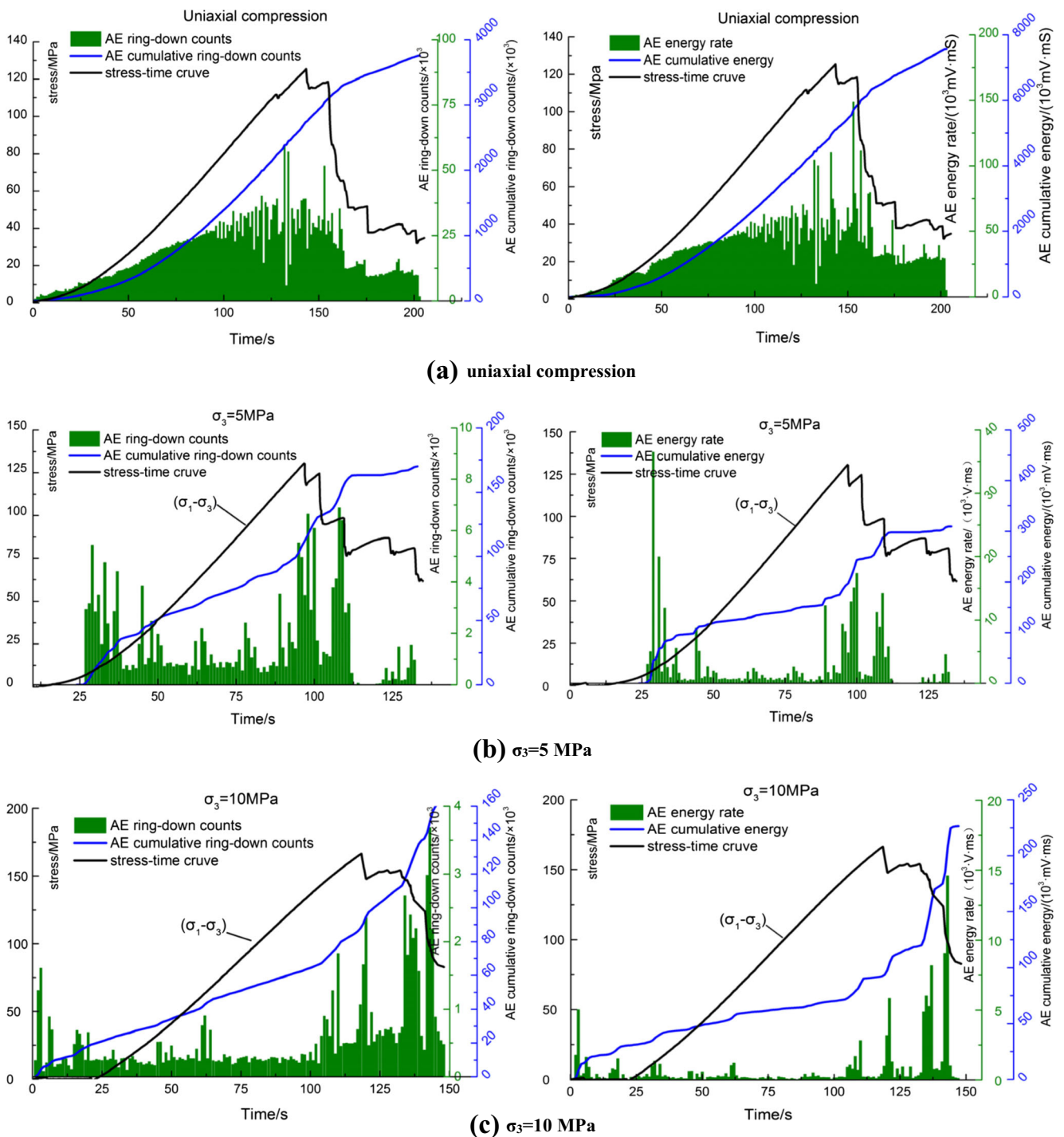
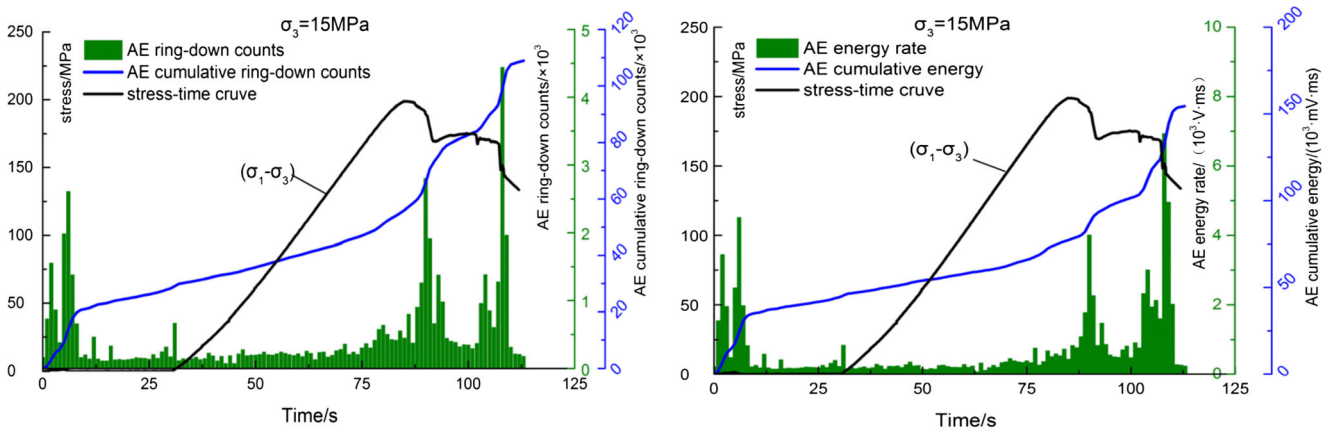


**Fig. 7** Acoustic emission ring-down counts and energy rates under different confining pressures

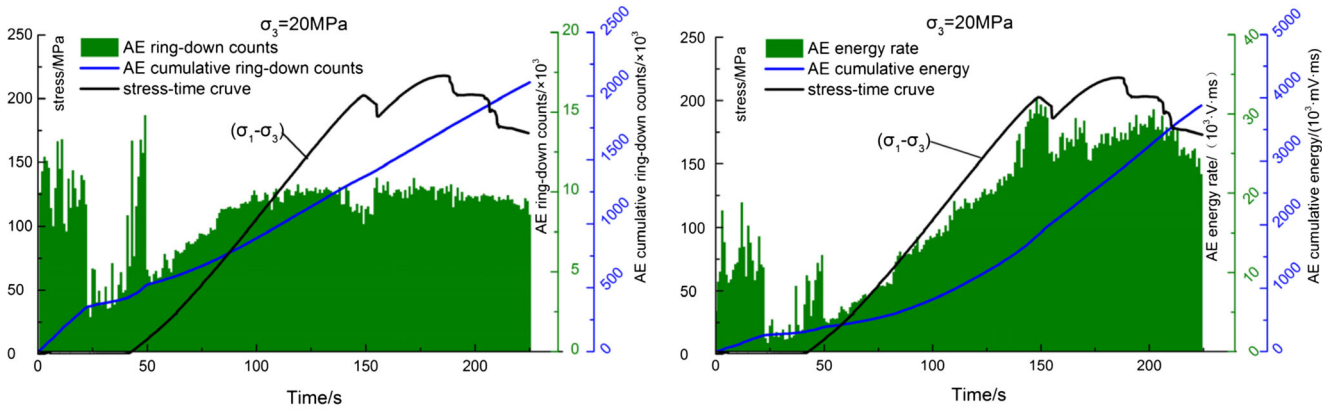
Ductility increases with increasing confining pressure. Confining pressure inhibits particle breakage and crack slippage during compression, thus increasing shear failure strength and post-peak carrying capacity. Yield stress and peak stress increase with confining pressure. As shown in Fig. 5, peak strength increases linearly with increasing confining pressure.

### Failure characteristics

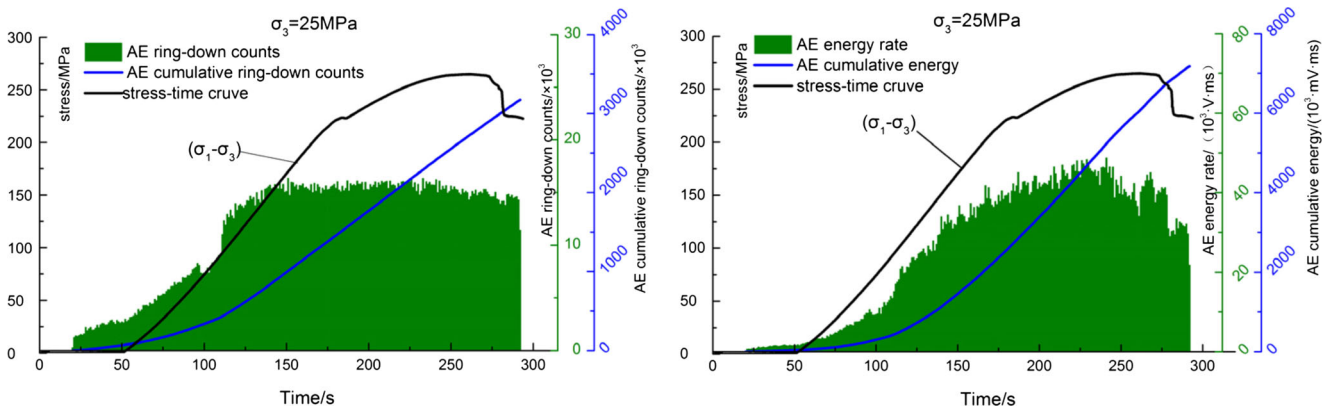
As shown in Fig. 3a, rock failure under uniaxial compression produces many longitudinal cracks in the loading direction. The failure surface is rough, which indicates tension destruction. As shown in Fig. 6, the rock produces a smooth fracture surface under triaxial



(d)  $\sigma_3=15$  MPa



(e)  $\sigma_3=20$  MPa



(f)  $\sigma_3=25$  MPa

Fig. 7 (continued)

compression, which indicates shear failure. When confining pressure is low, the macroscopic fracture surface is mainly shear failure, but local splitting damage is also present. The pattern of fracture indicates the presence of tension and twist. The fracture surface becomes increasingly smooth with increasing confining pressure,

and white powder is produced on the shear plane. The degree of fracture increases with increasing confining pressure, and this phenomenon is closely associated with energy absorption and release (which is discussed below in the section [Analysis of the energy mechanism](#)).

## Analysis of AE characteristics

AE technology is used to monitor rock failure in real-time. It uses the variation in the characteristics of parameters during the test. We studied the AE characteristics of saturated limestone under uniaxial and triaxial compression.

### AE ring-down counts and energy rate

As shown in Fig. 7, the tests revealed the rules governing the changes in AE ring-down counts and energy rates during the test. A detailed analysis and description are provided below.

The rock sample produces AE activity during the entire loading process under uniaxial compression. At the beginning of loading, the primary fractures close, and failure and friction of some fractures cause a small amount of AE activity. With the increase in stress, the sample enters the elastic stage, and the stress is insufficient to form new fractures. However, the slipping of some fractures produces AE activity at low levels. With continuous loading, the sample enters the fracture development stage, and the fractures begin to extend, new cracks form, and AE activity gradually increases. When the rock reaches the dilatancy stage, interaction among the cracks begins to intensify, and the fractures begin to coalesce, and macroscopic cracks gradually form. AE activity is highest before peak stress (Su et al. 2011). Confining pressure enhances the plasticity of the limestone. With increasing confining pressure, the post-peak curve of the limestone changes from strain softening to ideal plasticity. The AE characteristics of the limestone under triaxial compression are clearly different from those under uniaxial compression.

The changes in AE activity under triaxial compression can be summarized as follows:

1. Initial compaction stage: Confining pressure causes the primary fractures to close tightly, which increases the integrity and stiffness of the rock sample. AE activity decreases considerably more under triaxial compression than under uniaxial compression. Different levels of AE activity with high energy may exist because the limestone rock in the test contained many fractures, and some original internal cracks were not closed completely because of the low initial confining pressure. The original cracks close and cause AE activity with increasing stress, but the duration is short.
2. Elastic stage: The stress is insufficient to form new fractures, but the slipping of some fractures produces AE activity at low levels. As shown in Fig. 7, the AE activity increases slowly in the elastic stage under uniaxial

compression. Confining pressure enhances rock integrity and stiffness, and fractures can be considered stable

3. The sample enters the plastic stage when axial stress reaches its ultimate value. The inner fractures coalesce, the interaction among fractures increases, which enhances the AE activity. The AE peak under triaxial compression is slightly behind the stress peak, and it appears where the stress decreases sharply. This phenomenon is due to the binding constraint of confining pressure; the rock sample still has high bearing capacity at the stress peak, obvious friction and slide among blocks occurs in the process, and stress decreases sharply to the residual stress, which causes the AE peak to move backwards (Yang et al. 2014).
4. With increasing confining pressure, the AE characteristics of the limestone rock change significantly. When the confining pressure is less than 15 MPa, the maximum AE appears where the stress decreases sharply. When the confining pressure increases to 20 MPa, there is no obvious AE peak in the loading process. When  $\sigma_3 = 5$  MPa, the AE cumulative ring-down is  $1.70 \times 10^5$ , and when  $\sigma_3 = 15$  MPa, cumulative ring-down is  $0.98 \times 10^5$ , a decrease of about 60%. However, when the confining pressure is 20 MPa or 25 MPa, the AE activity is much larger than that under 15 MPa of confining pressure. So under triaxial compression, the AE activity of the rock first decreases and then increases with increasing confining pressure.

### Analysis of AE amplitude and ASL

As shown in Fig. 8, we studied the characteristics of AE amplitude and ASL during the loading process using AE tests. In the uniaxial compression tests, AE activity occurs during the entire loading process, and the AE ASL does not show stratification. In the triaxial compression tests, AE activity lags behind, and the AE amplitude is mainly in the range 50–75 mV and clear stratification of ASL occurs when the confining pressure is low ( $\sigma_3 < 15$  MPa). AE activities with high amplitude appear when the stress decreases sharply. With increasing confining pressure, the stratification of ASL disappears and the AE amplitude increases to 50–125 mV under high confining pressure ( $\sigma_3 > 20$  MPa). Therefore, the critical confining pressure that causes the AE characteristics of the limestone to change rapidly is between 15 and 20 MPa.

## Energy mechanism of saturated limestone

### Energy theory

Based on the energy conservation law, the energy theory of a unit volume of rock is described as follows (Xie et al. 2005, 2008):



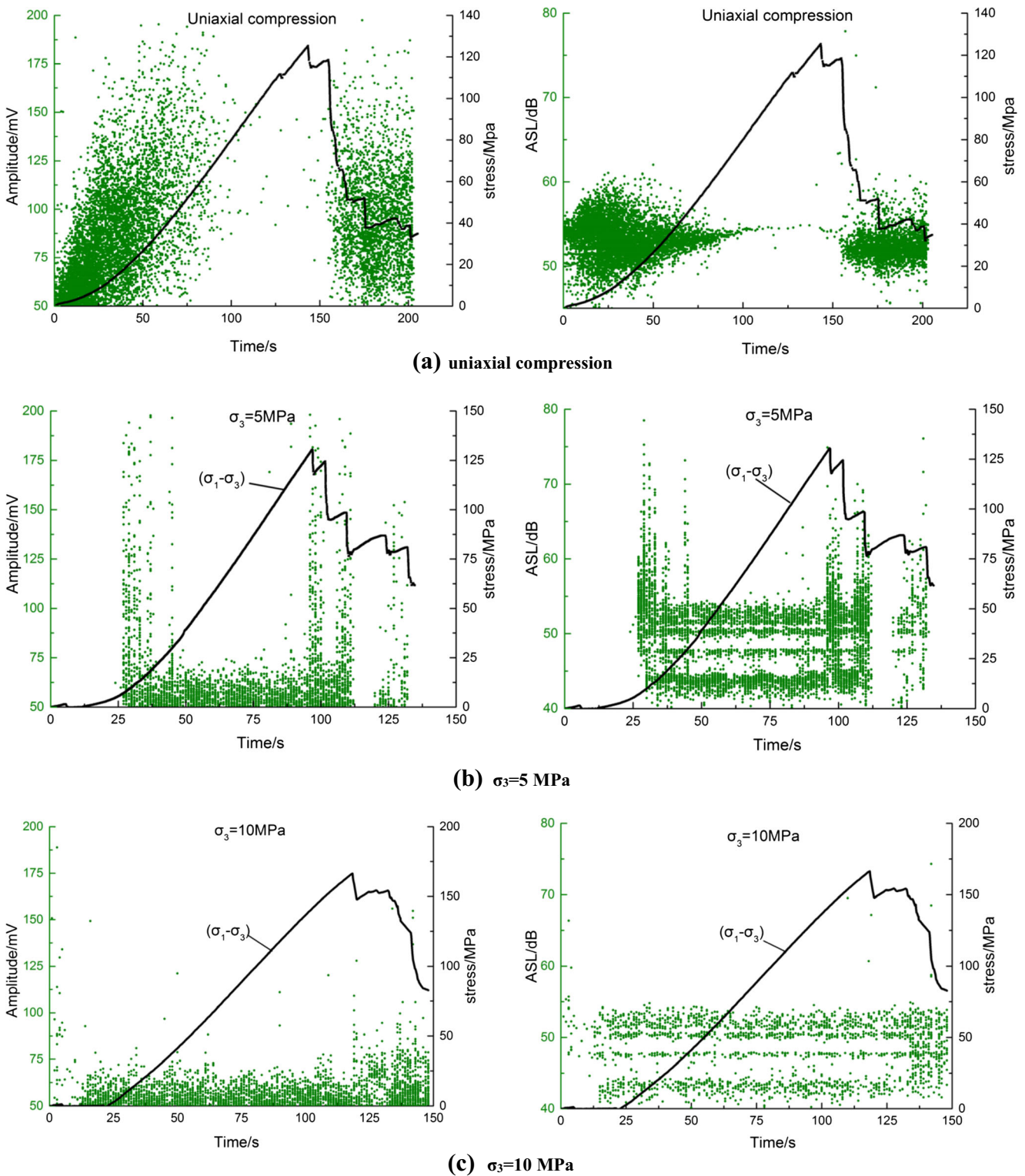


**Fig. 8** Characteristic of acoustic emission amplitude and average signal level (ASL) under different confining pressure

$$W = U = U^e + U^d \tag{1}$$

where  $W$  is the work done outside,  $U$  is the energy absorbed from outside,  $U^e$  is the freeable elastic strain energy, and  $U^d$  is the

dissipated energy. The relationship between  $U^e$  and  $U^d$  is shown in Fig. 9.

According to Xie et al. (2005), You and Hua (2002), and Huang et al. (2012), only axial stress acts on the rock under uniaxial compression:

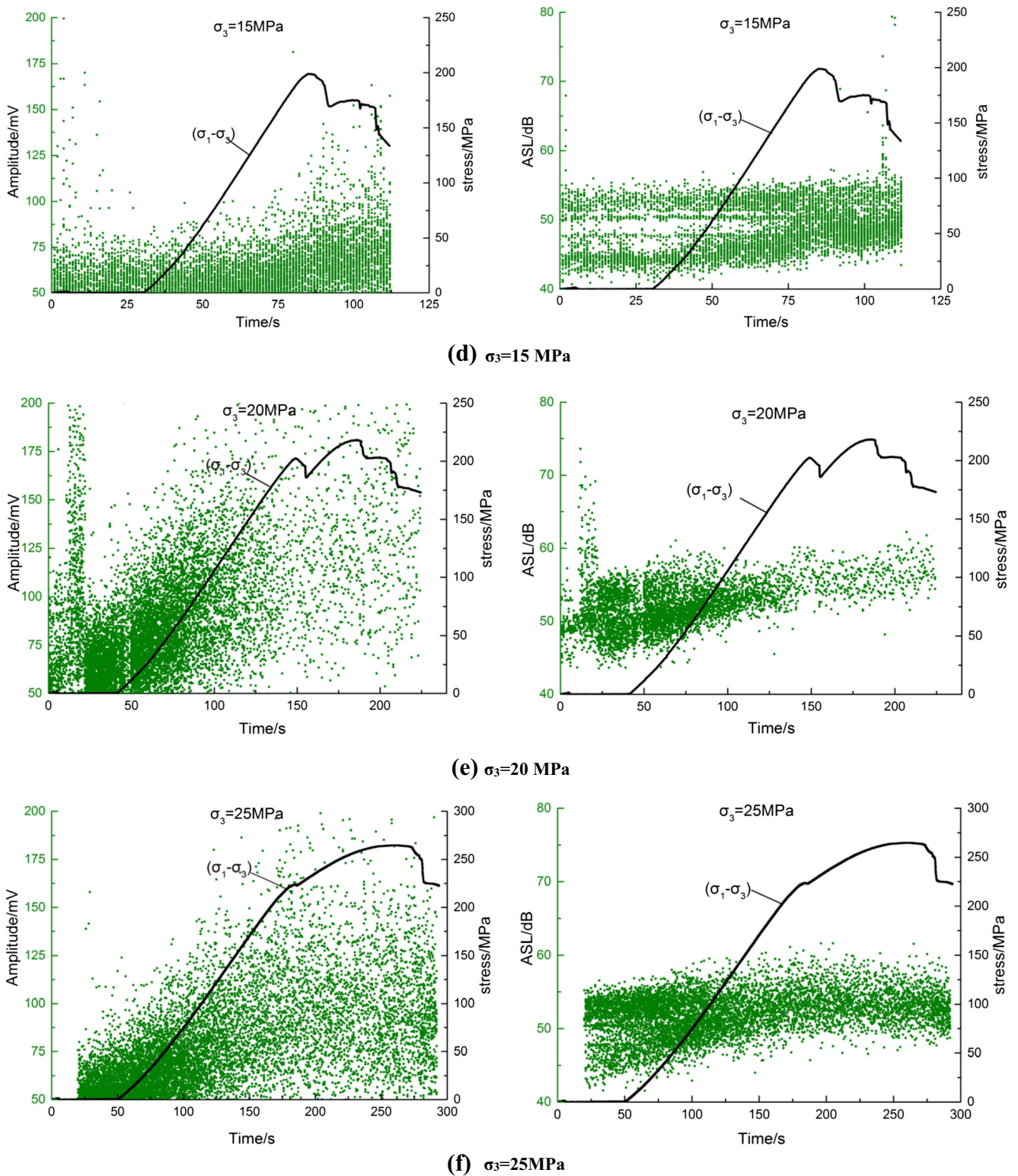


Fig. 8 (continued)

$$U = \int_0^{\epsilon_1} \sigma_1 d\epsilon_1 \tag{2}$$

$$U^e = \frac{1}{2E_i} \sigma_1^2 \approx \frac{1}{2E_0} \sigma_1^2 \tag{3}$$

where  $E_i$  is the unloading elastic modulus, and  $E_0$  is the initial elastic modulus. In the analysis  $E_i$  can be replaced by  $E_0$ .

Under triaxial compression, both axial stress and confining pressure act on the rock, and  $\sigma_2 = \sigma_3$ :

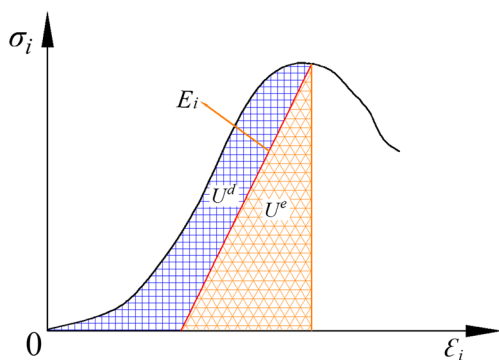


**Fig. 9** Relationship between  $U^e$  and  $U^d$

$$U = \int_0^{\varepsilon_1} \sigma_1 d\varepsilon_1 + 2 \int_0^{\varepsilon_3} \sigma_3 d\varepsilon_3 \quad (4)$$

$$U^e = \frac{1}{2E_i} [\sigma_1^2 + 2\sigma_3^2 - 2\mu(\sigma_3^2 + 2\sigma_1\sigma_3)] \approx \frac{1}{2E_0} [\sigma_1^2 + 2\sigma_3^2 - 2\mu(\sigma_3^2 + 2\sigma_1\sigma_3)] \quad (5)$$

$$U^d = U - U^e \quad (6)$$

Guo et al. (2014) considered that the amount of energy absorbed by the rock during the hydrostatic pressure stage is small and can be disregarded. Accordingly, the energy absorbed during the hydrostatic pressure stage was disregarded in the analysis of the energy mechanism in this study.

### Energy mechanism

Sample damage is the result of a process of macroscopic failure evolution driven by energy; it results from the combination of accumulation and transformation of dissipated energy and elastic energy. Dissipated energy can cause damage to rock leading to deterioration and loss of strength. Internal energy release is the reason for sudden rock failure (Guo et al. 2014). Figure 10 shows the laws governing the changes in strain energy and AE activity under different loading conditions.

1. Initial stage: The original cracks close. The rock sample absorbs mechanical energy from outside, and some of the energy is stored as elastic energy. The original cracks close; friction and slippage among the cracks consume energy and produce AE activity. AE activity with high energy may also be present because of the closure of original cracks.
2. Elastic stage: The original cracks are completely closed, and the energy input from outside is mainly used for elastic compaction; thus, most of the energy is transformed into elastic strain energy stored in the rock.
3. Stable stage of fracture growth: New fractures appear, so some of the energy is consumed as surface energy and

other forms of radiant energy; however, most of the energy is stored in the rock as elastic strain energy.

4. Unstable stage of fracture growth: The fractures extend to the rock surface, many cross-cracks gather, and fracture propagation enters an unstable stage. The proportion of elastic strain energy decreases, whereas that of dissipated energy increases significantly. In this stage active AE is often present.
5. Failure stage: The fractures link, and macroscopic cracks appear. The stored elastic strain energy is released and decreases sharply, accompanied by strong AE. Meanwhile, dissipated energy increases rapidly, and the rock divides into blocks of different sizes.

The analysis indicates that energy conversion during rock failure can be divided into three stages. The first is energy accumulation (including initial, elastic, and stable stages of fracture growth), in which the input energy is mainly converted into elastic strain energy. The second stage is energy dissipation (corresponding to the unstable stage of fracture growth), in which the proportion of elastic strain energy decreases, whereas that of dissipated energy increases significantly. The third stage is energy release (corresponding to the formation of macroscopic cracks and post-peak failure stage), in which the elastic strain energy is released as kinetic energy, radiation energy, and friction heat energy with strong AE activity. Internal elastic strain energy and dissipation energy are present in the entire process of rock deformation and failure. The ratios of the two energy types are different and changing; thus, the rock shows the characteristics of energy accumulation, dissipation, and release. The energy at the peak stress according to the test results is shown in Table 1 and Figs. 11 and 12.

As shown in Table 1, the total strain energy ( $U$ ), dissipation strain energy ( $U^d$ ), and elastic strain energy ( $U^e$ ) of the saturated limestone sample are all higher under triaxial compression than under uniaxial compression. With increasing confining pressure, the ratio of the maximum releasable strain energy ( $U^e$ ) decreases at peak stress, whereas the ratio of dissipated energy ( $U^d$ ) increases.

As shown in Fig. 11, the total energy ( $U$ ), dissipated energy ( $U^d$ ) and elastic strain energy ( $U^e$ ) at peak stress of the limestone samples have good exponential relationships with confining pressure. When confining pressure is low, the growth rate of  $U$  is slow; when  $\sigma_3 > 15$  MPa, the growth rate increases sharply. The ultimate strength of the rock increases gradually, and more energy from outside is required. When confining pressure is low, the growth rate of  $U^d$  is slow; when  $\sigma_3 > 20$  MPa, the growth rate increases sharply. With increasing confining pressure, plastic deformation before peak stress increases. The rock thus experiences a long period of plastic



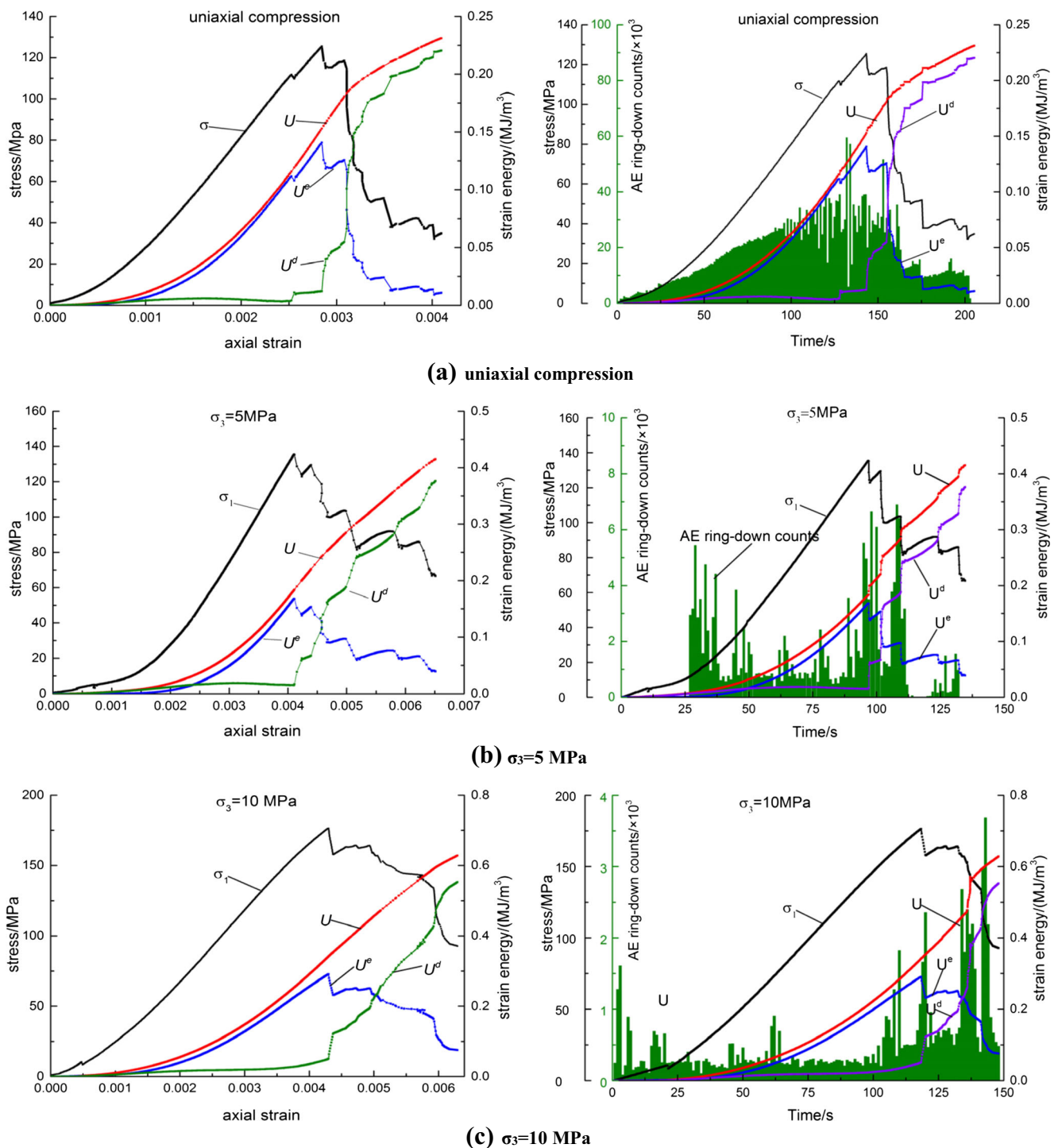


**Fig. 10** Characteristics of AE and strain energy under different confining pressures

flow failure.  $U^d$  and plastic deformation show a positive correlation. High confining pressure can prevent the storage of elastic energy. Considering the two aspects, dissipated energy increases with confining pressure, and the ratio of  $U^d$  to  $U$  also increases. When confining pressure is 25 MPa,  $U^d/U = 55.80\%$ ,  $U^d/U^e = 1.26$ , and  $U^d$  is larger than  $U^e$ .

As shown in Fig. 12, the total energy ( $U$ ), elastic strain energy ( $U^e$ ), and dissipation energy ( $U^d$ ) at peak stress increase with peak strength of the rock. When peak strength is low,  $U$  and  $U^d$  increase with  $\sigma_{peak}$  slowly; when  $\sigma_{peak}$  is larger than 250 MPa, the growth rates of  $U$  and  $U^d$  increase sharply.  $U$ ,  $U^d$  and  $U^e$  at peak stress show good exponential



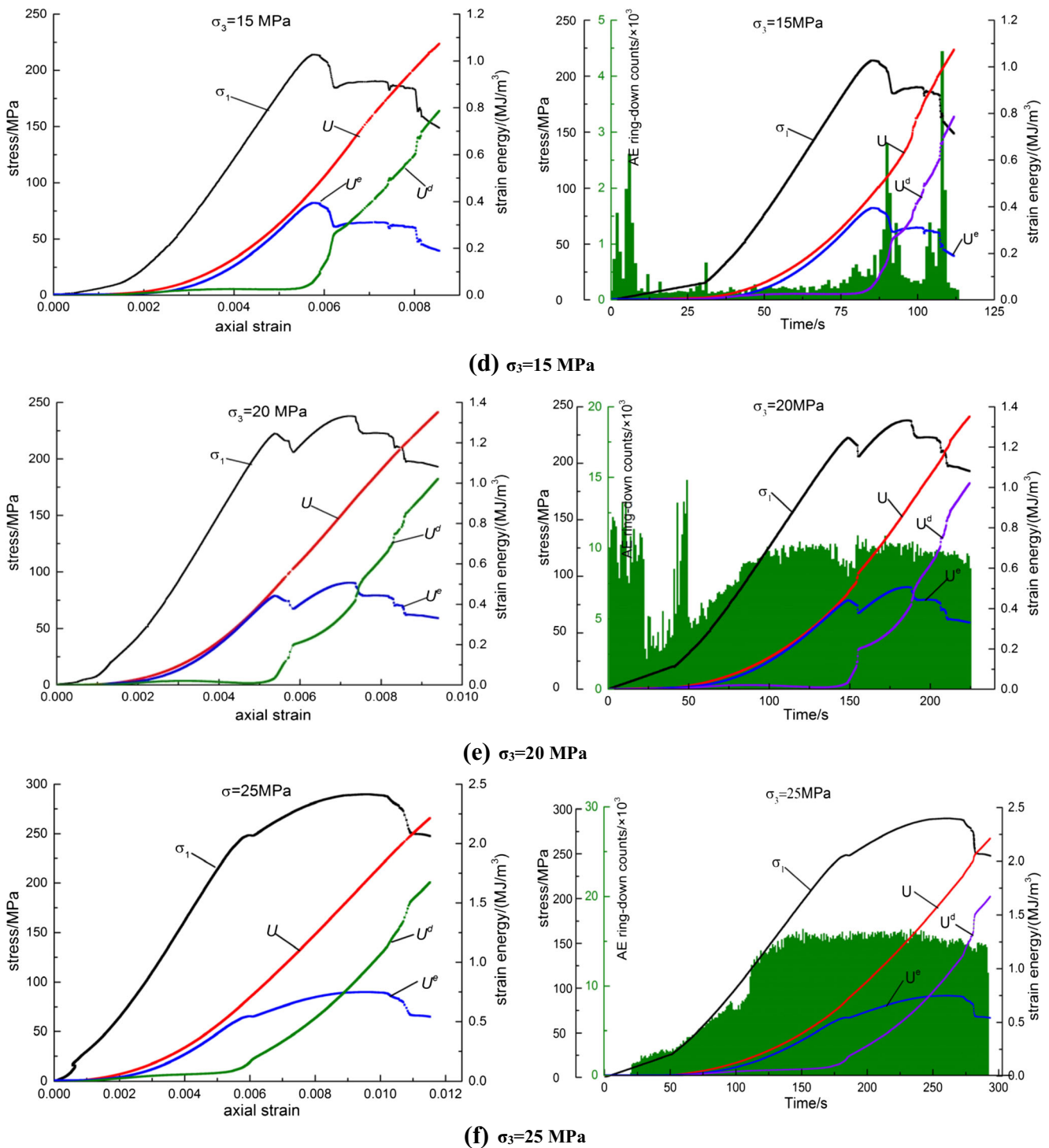


Fig. 10 (continued)

relationships with  $\sigma_{\text{peak}}$ . The square of the correlation coefficients are all larger than 0.95.

At the macro level, the energy is mainly stored as elastic strain energy in the early stage of rock deformation. The energy is then dissipated through rock damage. In the failure stage, the energy is mainly released sharply. At the microscopic level, many mechanisms cause strain hardening or strain

softening of the rock, and whether the energy will be stored or released depends on the final result of the energy competition mechanism. Regarding the energy-driven nature of rock failure, the difference in dissipated energy under different confining pressures inevitably leads to different failure modes. The dissipated strain energy under triaxial compression is clearly higher than that under uniaxial compression, which

**Table 1** Strain energy of saturated limestone at peak stress (where  $U$  is the total strain energy,  $U^d$  is the dissipation strain energy, and  $U^e$  is the elastic strain energy of the sample)

| Loading              |                     | $U$ (MJ/m <sup>3</sup> ) | $U^e$ (MJ/m <sup>3</sup> ) | $U^d$ (MJ/m <sup>3</sup> ) | $U^e/U$ | $U^d/U$ | $U^d/U^e$ |
|----------------------|---------------------|--------------------------|----------------------------|----------------------------|---------|---------|-----------|
| Uniaxial compression | $\sigma_3 = 0$ MPa  | 0.1668                   | 0.1549                     | 0.0119                     | 0.9287  | 0.0713  | 0.0768    |
|                      | $\sigma_3 = 0$ MPa  | 0.1841                   | 0.1830                     | 0.0011                     | 0.9940  | 0.0060  | 0.0060    |
|                      | $\sigma_3 = 0$ MPa  | 0.1529                   | 0.1407                     | 0.0122                     | 0.9202  | 0.0798  | 0.0867    |
| Triaxial compression | $\sigma_3 = 5$ MPa  | 0.1832                   | 0.1679                     | 0.0153                     | 0.9165  | 0.0835  | 0.0911    |
|                      | $\sigma_3 = 10$ MPa | 0.3417                   | 0.2908                     | 0.0509                     | 0.8511  | 0.1489  | 0.1750    |
|                      | $\sigma_3 = 15$ MPa | 0.5044                   | 0.3788                     | 0.1256                     | 0.7510  | 0.2490  | 0.3315    |
|                      | $\sigma_3 = 20$ MPa | 0.8999                   | 0.5425                     | 0.3564                     | 0.6036  | 0.3964  | 0.6569    |
|                      | $\sigma_3 = 25$ MPa | 1.6940                   | 0.7488                     | 0.9452                     | 0.4420  | 0.5580  | 1.2623    |

has an exponentially increasing relationship with confining pressure. With increasing confining pressure, the rock-fracturing mode is developed from the failure of a single shear plane with less energy consumption to more shear failure planes with more energy dissipation (Tian and Yu 2014).

The formulas from the regression analysis in Figs. 11 and 12 have the same form, which indirectly indicates that the peak stress of rock samples has a linear relationship with confining pressure, and also confirms the result shown in Fig. 5.

## Discussion

1. In the experiments, the confining pressure in the triaxial compression tests was provided by hydraulic fluid. The rock specimen was wrapped in rubber, and the hydraulic fluid and triaxial cylinder were outside the rubber. Therefore, the sensors were not in direct contact with the rock sample. The faint initial AE signals occurring during initial loading might be difficult to receive because of the attenuation of the rubber, hydraulic fluid, and cylinder. However, the strong AE signals occurring during the yielding stage and macroscopic fracture stage are little affected, so there is a minimal effect on the qualitative analysis of AE characteristics during rock failure (Su et al. 2011). Yang et al. (2014) found that under the same experimental conditions, the maximum values of AE ring-down counts and test energy when the detectors are inside the triaxial cell are, respectively, 27% and 32% higher than the values obtained when the detectors are outside. The tests showed that the peak AE ring-down counts under uniaxial compression is more than 10 times that under low confining pressure, and the cumulative AE ring-down counts under uniaxial compression are more than 20 times those under low confining pressure. Considering the absorbing effect of the hydraulic fluid and cylinder wall, AE activity remains significantly stronger under uniaxial compression than under low confining pressure. When there is no confining pressure, the internal cracks grow rapidly, and the AE activity is intense during rock failure.

2. Guo et al. (2014) found that the strain energy of karst limestone at peak stress under natural and saturated conditions increases linearly with confining pressure. In the current study, total strain energy ( $U$ ) and dissipated strain energy ( $U^d$ ) at peak stress show an exponential growth relationship with confining pressure. Guo et al. (2014) found a maximum confining pressure of 20 MPa, whereas the maximum confining pressure in the current study was 25 MPa. The experimental results indicate that when confining pressure is less than 20 MPa, the relationship between strain energy and confining pressure is approximately linear. When confining pressure increases from 20 MPa to 25 MPa, the total strain energy ( $U$ ) and dissipated strain energy ( $U^d$ ) increase sharply (the former increased from 0.8999 MJ/m<sup>3</sup> to 1.6940 MJ/m<sup>3</sup>, an increase of about 100%, and the latter increased from 0.3564 MJ/m<sup>3</sup> to about 0.9452 MJ/m<sup>3</sup>, and increase of about 200%). The curve-fitting results show an exponential growth relationship.
3. Many scholars have studied the laws governing the changes in AE fractal characteristics and fractal dimension values in the rock failure process and established rock strength fractal models through AE tests (Wu et al.

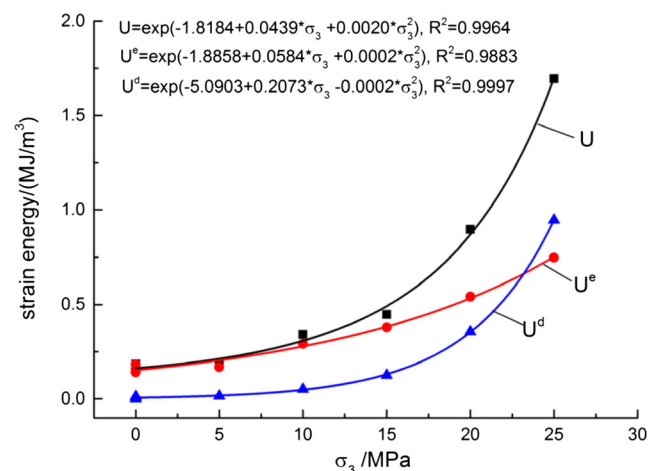


**Fig. 11** Relationship between strain energy and confining pressure

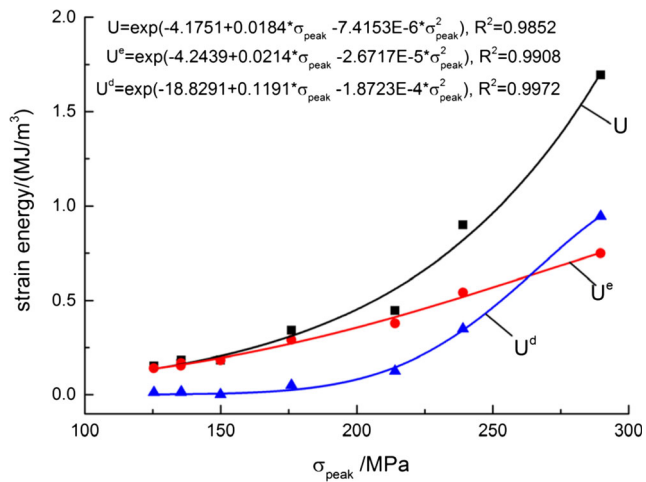


Fig. 12 Relationship between strain energy and peak stress

2012; Zhou and Liu 2010). These studies indicate that the continued reduction in AE fractal dimension values is a sign of rock failure. Therefore, further study of the four aspects of karst limestone, namely mechanical properties, AE characteristics, fractal features, and energy characteristics, is necessary.

## Summary

1. Brittle failure of saturated limestone is intense under uniaxial compression. It is related to tension destruction and shows connection of longitudinal cracks. Under triaxial compression, yield stress and peak strength increase with increasing confining pressure, and the post-peak stress curve of limestone changes to ideal plasticity from strain softening. The rock produces a shear plane under triaxial compression, which is related to shear failure. With increasing confining pressure, the rock failure mode develops from a single shear plane with low energy consumption to more shear failure planes with high energy dissipation.
2. AE activity under triaxial compression differs from that under uniaxial compression. The rock sample produces AE activity during the entire loading process under uniaxial compression, which gradually increases in strength with the increase in stress. AE activity is most powerful before peak stress. Under triaxial compression, confining pressure causes the primary fractures to close tightly, which increases the integrity and stiffness of the rock sample. The AE peak appears with a sharp stress decrease and rock macroscopic failure.
3. With increasing confining pressure, the AE characteristics of limestone change significantly. Under triaxial compression, the AE activities of the rock decrease first then

increase with increasing confining pressure. When the confining pressure is less than 15 MPa, intermittent peaks exist, and the maximum of AE appears where the stress decreases sharply. When the confining pressure increases to 20 MPa, no obvious AE peaks emerge during the loading process. Considering the AE amplitude and ASL characteristics, the amplitudes are mainly in the range 50–75 mV and a clear stratified phenomenon appears when the confining pressure is low ( $\sigma_3 < 15$  MPa). The AE amplitude increases to 50–125 mV and the stratified phenomenon disappears under high confining pressures ( $\sigma_3 > 20$  MPa). Accordingly, the critical confining pressure is between 15 and 20 MPa, and it causes a dramatic change in the AE characteristics of the limestone.

4. Energy conversion stages in rock during the loading process can be divided into accumulation, dissipation, and release. AE is a part of the dissipation energy, which is strong in the energy release stage. The regression analysis shows that the total energy ( $U$ ), dissipated energy ( $U^d$ ), and elastic energy ( $U^e$ ) at peak stress show a good exponential relationship with confining pressure and peak strength.

**Acknowledgements** This work was financially supported by the State Key Development Program for Basic Research of China (grant no. 2013CB036003) and the National Natural Science Foundation of China (grant no. 51778215). The authors thank the reviewers of this paper for their constructive comments and suggestions for its improvement. All the authors declare that there is no conflict of interest regarding the publication of this paper.

## References

- Amitrano D (2003) Brittle-ductile transition and associated seismicity: experimental and numerical studies and relationship with the  $b$  value. *J Geophys Res* 108(B1). <https://doi.org/10.1029/2001JB000680>
- Brantut N, Schubnel A, Gueguen Y (2011) Damage and rupture dynamics at the brittle-ductile transition: the case of gypsum. *J Geophys Res Solid Earth* 116(B1). <https://doi.org/10.1029/2010JB007675>
- Chen W, Konietzky H, Tan X, Fruhwirt T (2016) Pre-failure damage analysis for brittle rocks under triaxial compression. *Comput Geotech* 74:45–55. <https://doi.org/10.1016/j.compgeo.2015.11.018>
- Farahat AM, Ohtsu M (1995) Evaluation of plastic damage in concrete by acoustic emission. *J Mater Civ Eng* 7(3):148–153. [https://doi.org/10.1061/\(ASCE\)0899-1561\(1995\)7:3\(148\)](https://doi.org/10.1061/(ASCE)0899-1561(1995)7:3(148))
- Guo JQ, Liu XL, Qiao CS (2014) Experimental study of mechanical properties and energy mechanism of karst limestone under natural and saturated states. *Chin J Rock Mech Eng* 33(2):296–308. [13722/j.cnki.jme.2014.02.005](https://doi.org/10.13722/j.cnki.jme.2014.02.005)
- Huang D, Li YR (2013) Conversion of strain energy in triaxial unloading tests on marble. *Int J Rock Mech Min Sci* 66:160–168. <https://doi.org/10.1016/j.ijmmms.2013.12.001>
- Huang D, Huang RQ, Zhang YX (2012) Experimental investigations on static loading rate effects on mechanical properties and energy mechanism of coarse crystal grain marble under uniaxial compression. *Chin J Rock Mech Eng* 31(2):245–255
- Iturrioz I, Lacidogna G, Carpinteri A (2013) Experimental analysis and truss-like discrete element model simulation of concrete specimens

- under uniaxial compression. *Eng Fract Mech* 110:81–98. <https://doi.org/10.1016/j.engfracmech.2013.07.011>
- Iturrioz I, Lacidogna G, Carpinteri A (2014) Acoustic emission detection in concrete specimens: experimental analysis and lattice model simulations. *Int J Damage Mech* 23(3):327–358. <https://doi.org/10.1177/1056789513494232>
- Lee B, Rathnaweera TD (2016) Stress threshold identification of progressive fracturing in Bukit Timah granite under uniaxial and triaxial stress conditions. *Geomech Geophys Geo-Energy Geo-Resources* 2(4):301–330. <https://doi.org/10.1007/s40948-016-0037-z>
- Li CS, Liao YK, Gu T (2007) Preliminary study on mechanical property tests for karst rock. *Chin J Undergr Space Eng* 3(7):1358–1362+1386
- Li YR, Huang D, Li X (2014) Strain rate dependency of coarse crystal marble under uniaxial compression: strength, deformation and strain energy. *Rock Mech Rock Eng* 47(4):1153–1164. <https://doi.org/10.1007/s00603-013-0472-x>
- Liu XX, Liang ZZ, Zhang YB et al (2015) Acoustic emission signal recognition of different rocks using wavelet transform and artificial neural network. *Shock Vib* 2015:846308. <https://doi.org/10.1155/2015/846308>
- Lokajicek T, Prikryl R, Rudajev V (1996) Energy-frequency distribution of acoustic emission from loaded rock samples. *Mater Sci Forum* 210-213:541–548
- Mikhalyuk AV, Zakharov VV (1997) Dissipation of dynamic-loading energy in quasi-elastic deformation processes in rocks. *J Appl Mech Tech Phys* 38(2):312–318. <https://doi.org/10.1007/BF02467918>
- Prikryl R, Lokajicek T, Li C, Rudajev V (2003) Acoustic emission characteristics and failure of uniaxially stressed granitic rocks: the effect of rock fabric. *Rock Mech Rock Eng* 36(4):255–270. <https://doi.org/10.1007/s00603-003-0051-7>
- Su CD, Zhai XX, Li BF (2011) Experimental study of the characteristics of acoustic emission for sandstone specimens under uniaxial and triaxial compression tests. *J Min Saf Eng* 28(2):225–230
- Tang Q, Li YN (2014) Influence of confining stress on energy evolution of sandstone under triaxial compression. *Electron J Geotech Eng* 19N:3159–3165
- Tian Y, Yu RG (2014) Energy analysis of limestone during triaxial compression under different confining pressures. *Rock Soil Mech* 35(1):118–122. [10.16285/j.rsm.2014.01.019](https://doi.org/10.16285/j.rsm.2014.01.019)
- Tuncay E, Obara Y (2012) Comparison of stresses obtained from acoustic emission and compact conical-ended borehole overcoring techniques and an evaluation of the Kaiser effect level. *Bull Eng Geol Environ* 71(2):367–377. <https://doi.org/10.1007/s10064-011-0362-y>
- Vervoort A, Govaerts A (2006) Kaiser effect in tri-axial tests of limestone samples. *Proc Monogr Eng Water Earth Science* 2006:143–149. <https://doi.org/10.1201/9781439833650.ch19>
- Wang DC, Wang K, Zhao NN (2014) Experimental study on time series characteristics of rock acoustic emission in complete stress-strain process under uniaxial compression. *Adv Mater Res* 243:2239–2244. <https://doi.org/10.4028/www.scientific.net/AMR.243-249.223>
- Wu XZ, Liu XX, Liang Z et al (2012) Experimental study of fractal dimension of AE serials of different rocks under uniaxial compression. *Rock Soil Mech* 33(12):3561–3569. [10.16285/j.rsm.2012.12.015](https://doi.org/10.16285/j.rsm.2012.12.015)
- Xiao YQ, Wan YP, Liu BX (2013) Research on landscape limestone damage and deformation under uniaxial compression. *Appl Mech Mater* 423:914–919. <https://doi.org/10.4028/www.scientific.net/AMM.423-426.914>
- Xie HP, Ju Y, Li LY (2005) Criteria for strength and structural failure of rocks based on energy dissipation and energy release principles. *Chin J Rock Mech Eng* 24(17):3003–3010
- Xie HP, Ju Y, Li LY, Peng RD (2008) Energy mechanism of deformation and failure of rock masses. *Chin J Rock Mech Eng* 27(9):1729–1740
- Yang HQ, Zhou XP (2010) Experimental investigation of damage evolution of Huanglong limestone under uniaxial compression. *Chin Civil Eng J* 43(5):117–123. [10.15951/j.tmgcxb.2010.05.013](https://doi.org/10.15951/j.tmgcxb.2010.05.013)
- Yang YJ, Wang DC, Guo MF, Li B (2014) Study of rock damage characteristics based on acoustic emission tests under triaxial compression. *Chin J Rock Mech Eng* 33(1):98–104. [10.13722/j.cnki.jrme.2014.01.008](https://doi.org/10.13722/j.cnki.jrme.2014.01.008)
- You MQ, Hua AZ (2002) Energy analysis of failure process of rock specimens. *Chin J Rock Mech Eng* 21(6):778–781
- Zhang ZZ, Gao F (2012) Research on nonlinear characteristics of rock energy evolution under uniaxial compression. *Chin J Rock Mech Eng* 31(6):1198–1207
- Zhang LM, Gao S, Wang ZQ (2013) Experimental study of energy evolution of limestone underloading and unloading conditions. *Rock Soil Mech* 34(11):3071–3076. [10.16285/j.rsm.2013.11.004](https://doi.org/10.16285/j.rsm.2013.11.004)
- Zhou XP, Liu QY (2010) Research on chaotic characteristics of rock acoustic emission. *Rock Soil Mech* 31(3):815–819. [10.16285/j.rsm.2010.03.056](https://doi.org/10.16285/j.rsm.2010.03.056)